Liquefaction resistance of saturated and partly saturated clean sand under scenario earthquakes: numerical investigations

DHANAJI CHAVAN*[ID], THALLAK G SITHARAM and P ANBAZHAGAN

Department of Civil Engineering, Indian Institute of Science, Bangalore 560 012, India
e-mail: dschavan83@gmail.com; sitharam@iisc.ac.in; anbazhagan@iisc.ac.in

Abstract. Over last few years, induced desaturation is being considered as a new cost effective and environment friendly liquefaction mitigation technique. The present study investigates the effect of partial saturation on the liquefaction resistance of the soil domain. Three degrees of saturation were considered: 99%, 89.5% and 81.4%. Different thickness and position of the partly saturated zone were considered. A two-dimensional finite element model of soil ground of thickness of 30 m was subjected to four earthquake records from India. For fully saturated condition, increase in the permeability: (a) reduced magnitude of excess pore pressure, (b) increased rate of pore pressure dissipation and (c) increased acceleration at the ground surface. Investigation revealed that thickness of the partly saturated zone, with the degree of saturation of 81.4%, can be kept between 5 m to 15 m to prevent liquefaction under strong to very strong earthquakes having peak acceleration between 0.10 g to 0.36 g. Amplification factor at the ground surface for the degree of saturation of 81.4% was found to be in the range of 0.32 to 1.76. This implies that desaturation of clean sand up to the degree of saturation of 80% is enough to achieve the two-fold goal: (1) to prevent liquefaction and (2) to keep the acceleration amplification low. Residual lateral displacement was found to be a function of the degree of saturation, thickness and position of the partly saturated zone and input motion. Further reduction in the degree of saturation may amplify motion significantly owing to the presence of high matric suction, though this issue needs further investigation.

Keywords. Degree of saturation; Liquefaction; Pore pressure ratio; Amplification; Finite element.

1. Introduction

Earthquake is one of the major natural calamities which many times results in damage to both infrastructure and human life. One of the major devastating consequences of earthquakes is liquefaction of the soil. Quite a few techniques such as deep dynamic compaction, compaction grouting, explosive compaction, deep soil mixing etc., have been employed to prevent or minimize the liquefaction menace [1].

A technique called as induced desaturation is being looked at as a new liquefaction mitigation technique over last few years [2–7]. In this technique, degree of saturation of the soil is lowered by injecting/generating air/gas into the originally saturated soil [8, 9]. It was observed from the Shaking table and Centrifuge studies that desaturation prevented liquefaction [4, 9]. Further, footings resting on the desaturated soil bed underwent significantly smaller settlement than their saturated counterpart [5, 7, 10]. He *et al* [11] noted that undrained shear strength of the microbially desaturated loose clean sand got doubled when

degree of saturation was lowered by 10%. Further, they found that on desaturation, stress-strain response during triaxial compression changed from strain softening to strain hardening.

Pietruszczak *et al* [3] conducted numerical simulations for sand containing occluded air bubbles. They considered the degree of saturation in the range of 87% to 100% and found that fully saturated soil liquefied but partly saturated soil of a degree of saturation of 95% did not liquefy under the same earthquake loading. They proposed that induced desaturation can be considered as a possible liquefaction technique if we are successful somehow to inject air into the liquefaction prone saturated soil. Further, Okamura *et al* [8] simulated in-situ air injection using software TOUGH2. They recommended that this software was capable of simulating air-water interaction and flow. Marsini and Okamura [12] performed finite element simulation of centrifuge tests for desaturated soil supporting light structures. They found that excess pore water pressures and footing settlements obtained from the simulation were compared with those from centrifuge tests. Zhang *et al* [13] simulated stress controlled undrained cyclic triaxial tests using coupled hydro-mechanical constitutive model and found that

---

the effect of desaturation was predominant when a degree of saturation was just below 100%.

Noteworthy research has been carried out so far on induced desaturation. However, the performance of the soil domain with different degrees of saturation under scenario earthquakes is yet to be investigated. In the present study, numerical analysis has been carried out to understand the effect of degree of saturation, thickness and position of partly saturated zone and input motion on liquefaction resistance of a soil domain. The numerical investigation was performed employing open-source finite element software "OpenSees" developed by Pacific Earthquake Engineering Research (PEER) Center, University of California, Berkeley.

The poorly graded fine sand of relative density of 40% is considered in the analysis. Its index properties are: specific gravity 2.65, e_{max} 0.84, e_{min} 0.45, mean diameter (D_{50}) 0.27 mm and coefficient of uniformity (C_u) 2.14. Three degrees of saturation were considered: 99%, 89.5% and 81.4%. Samples were prepared by adopting dry deposition method. This was followed by saturation and desaturation [14] . In the end of desaturation, degree of saturation was computed from measured Skempton's B parameter. Then undrained cyclic triaxial tests were conducted on the specimen of above mentioned degrees of saturation. The experimental responses of these tests were then used to evaluate the constitutive parameters for the material model.

2. Finite element modeling of triaxial specimen

2.1 *Modelling triaxial specimen as a single BrickUP element*

The triaxial test is an element test [15]. As per the definition of the element test, the state of stress and strain at any point in the triaxial specimen is assumed to be the same [16]. Therefore, while modelling the triaxial specimen, it is essential to model the state of stress correctly, and the size of the finite element domain is immaterial [17]. The schematic explaining state of stress for the triaxial specimen is shown in figure 1. In figure 1a, σ_a is the axial stress which is sum of the confining stress σ_c and deviatoric stress σ_d. Free body diagram for a cubical element from the body of triaxial specimen is shown in Fig. 1b. In figure 1b, σ_1, σ_2 and σ_3 are major, intermediate and minor principal stress, respectively. Further, in conventional triaxial test $\sigma_2 = \sigma_3 = \sigma_c$. Thus, a triaxial specimen can be modeled as a single brick element with stress system shown in figure 1b. In the present study, triaxial test has been simulated employing BrickUP element in the OpenSees.

2.1.1 *About the "BrickUP" element*   It is an eight-node linear isoparametric hexahedral element entitled as "BrickUP" in the OpenSees. Each node has four degrees of

freedom; the first three are translational degrees of freedom for the solid skeleton, and the fourth one is pore fluid pressure, as shown in figure 1c. This element captures the undrained response of solid-fluid fully coupled material based on Biot's theory of poroelasticity [18]

2.2 *Boundary conditions and application of the confining pressure*

Utmost care must be taken while defining boundary conditions. It was observed from the trial simulations that even a small mistake in the application of the boundary condition either gives weird results or results in the failure of the simulation. The correct boundary conditions at each node during *consolidation* and *undrained monotonic/cyclic* loading are given in Table 1 and Table 2, respectively. The meaning of boundary conditions is as follow: a) for translational dof- *fixed* means zero displacement in a given direction and *free* means free to move in the given direction b) pore pressure: *fix* means drained condition and *free* means undrained condition.

Further, confining pressure was first converted into equivalent force. Then this equivalent force was applied as a nodal force, as shown in figure 2. The direction of application of the equivalent nodal force is given by arrows in figure 2.

2.3 *Application of monotonic and cyclic loading*

In the present study, strain controlled monotonic tests were conducted. These tests have been simulated by defining a strain rate of 0.6 mm/min at the top nodes of the BrickUP element. Strain rate can be defined at each node independently or node 8 can be connected with node 5, 6, 7 with an equal degree of freedom constraint in vertical direction and strain rate can be defined at node 8 only. Either procedure give the same result.

Cyclic triaxial tests have been simulated by applying sinusoidal deviatoric stress at the top nodes in the vertical direction (z direction) at a frequency of 0.1 Hz, unless otherwise specified. Before applying a cyclic load, top nodes were tied with equal degree freedom constraint in the vertical direction. This mimics the uniform vertical displacement of the top of the triaxial specimen observed in laboratory study.

2.4 *Stages in the analysis*

The analysis comprises three main stages. (1) *Gravity Analysis-Elastic*: self-weight and confining pressure is applied, and analysis is run with the constitutive model in linear elastic mode. (2) *Gravity Analysis-Elastic Plastic*: The constitutive model is switched to the elastic-plastic mode and analysis is run for few pseudo times steps. This
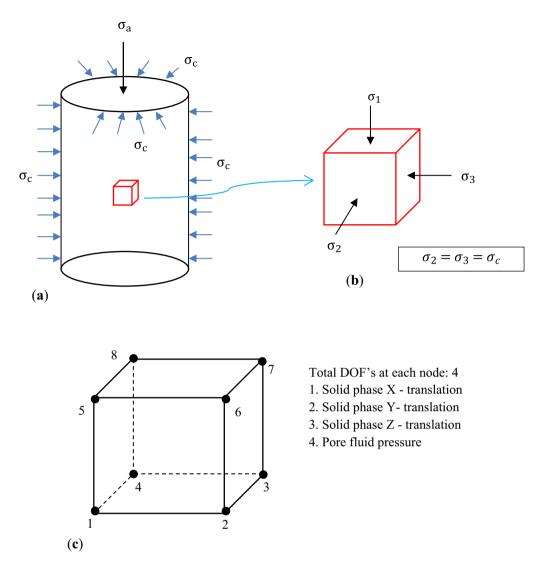
Figure 1. **a** schematic of triaxial specimen, **b** state of stress in a triaxial specimen and **c** connectivity and degree of freedom details for BrickUP element.

Table 1. Boundary conditions during consolidation

Node No.	DOF-1	DOF-2	DOF-3	DOF-4
1	Free	Fixed	Fixed	Fixed
2	Free	Free	Fixed	Fixed
3	Fixed	Free	Fixed	Fixed
4	Fixed	Fixed	Fixed	Fixed
5	Free	Fixed	Free	Fixed
6	Free	Free	Free	Fixed
7	Fixed	Free	Free	Fixed
8	Fixed	Fixed	Free	Fixed

Table 2. Boundary conditions during undrained monotonic/cyclic loading

Node No.	DOF-1	DOF-2	DOF-3	DOF-4
1	Free	Fixed	Fixed	Free
2	Free	Free	Fixed	Free
3	Fixed	Free	Fixed	Free
4	Fixed	Fixed	Fixed	Free
5	Free	Fixed	Free	Free
6	Free	Free	Free	Free
7	Fixed	Free	Free	Free
8	Fixed	Fixed	Free	Free

step is essential to adjust the state of stress given by step 1 on or within the outermost yield surface [19]. (3) *Monotonic/Dynamic Analysis-Elastic Plastic*: Constitutive material is in elastic-plastic mode and monotonic/cyclic load is applied.
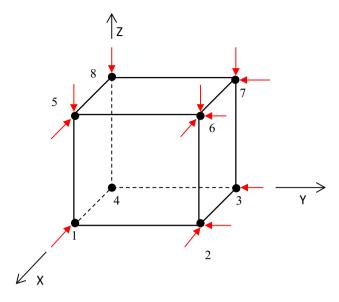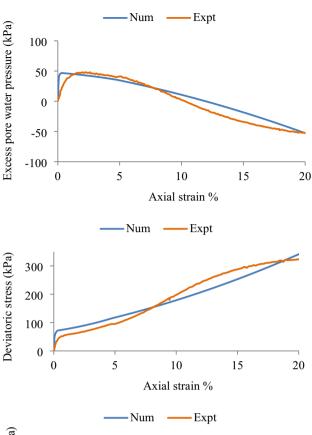
Figure 2. Application of confining pressure.

2.5 *Analysis objects*

In OpenSees, various components which are responsible for performing numerical analysis are called as analysis objects. These objects do various role such as storing the system of equations, setting the convergence criteria, solving the set of nonlinear equations, applying boundary conditions etc. The analysis objects employed in the present study, along with their role, are given in Table 3. The time step used in the analysis was 500 sec for static analysis. For dynamic analysis, it varied from 0.0025 to 0.01 sec. A detailed discussion about these analysis objects can be found in the OpenSees Command Language manual [20].

3. About the constitutive model

The stress-strain response of the sand has been modeled by pressure dependent multi yield material model entitled as "PressureDependMultiYield" in OpenSees. This model simulates the shear induced volume contraction and dilation, i.e., dilatancy and cyclic mobility observed for sandy
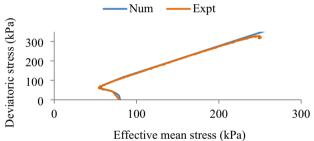

Figure 3. Dilatancy parameters for D_r 40, **S** 99, σ'_c 80 kPa: Comparison between experimental and numerical response after finalizing the dilatancy parameters:(*contrac* 0.4, *dilat1* 0.010 and *dilat2* 0.2).

soil under general loading conditions. The dilatancy is captured by following parameters: *contrac*, *dilat1*, *dilat2*. The parameter *contrac* is a nonnegative constant which

Table 3. Analysis objects employed in the present study

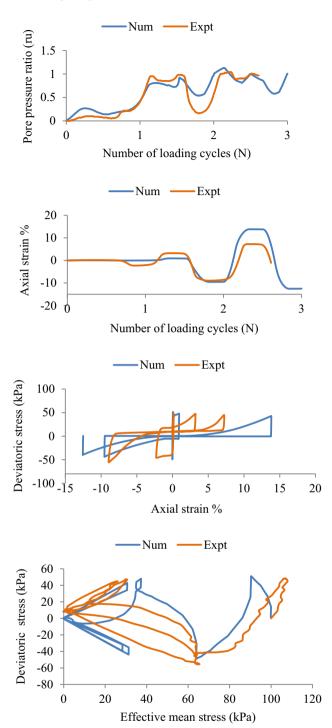| Object	Role	Name of Employed Object
System	How the system of equations in the analysis are stored and solved	ProfileSPD
Constraints	To enforce constraint equations in the analysis	Penalty
Test	Defines convergence criteria at the end of each iteration	NormDispIncr
Algorithm	This defines steps followed to solve non-linear equations	KrylovNewton
Numberer	How the degrees of freedom are numbered	RCM
Integrator	To perform numerical integration	Newmark
Analysis	Type of analysis: static/transient	Transient

Figure 4. Cyclic mobility parameters for D_r 40, **S 99**, σ'_c 100 kPa: cyclic mobility parameters - *liquefac1* 10, *liquefac2* 0.02, *liquefac3* 1.0.

defines the rate of shear-induced volume decrease in drained loading and rate of pore pressure build-up in undrained loading. Larger is the value, faster is the generation of pore pressure. Parameters *dilat1*, *dilat2*, are non-negative constants which define the rate of shear induced volume increase in drained loading and rate of pore
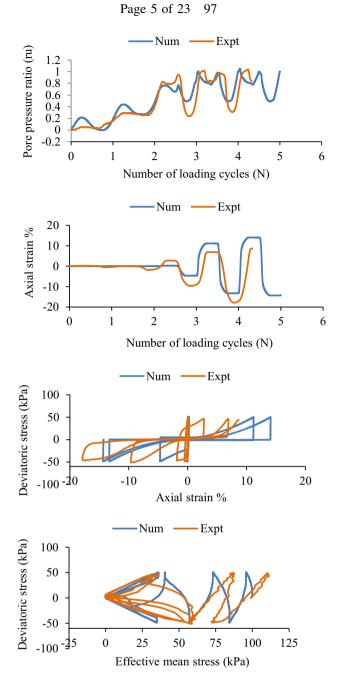

Figure 5. Comparison between experimental and numerical response for *S* 89.5, D_r 40, σ'_c 100 kPa (*contrac* 0.2, *dilat1* 0.01, *dilat2* 0.2).

pressure decrease in undrained loading due to dilative tendency. Larger value of these two parameters stands for faster reduction in the pore pressure. Axial straining corresponding to cyclic mobility is captured by following parameters: *liquefac1*, *liquefac2*, *liquefac3*. The parameter *liquefac1* defines the effective confining pressure below which the cyclic mobility mechanism is in effect. The parameter *liquefac2* defines the maximum amount of perfectly plastic shear strain developed at zero effective confinement during each loading phase. The parameter
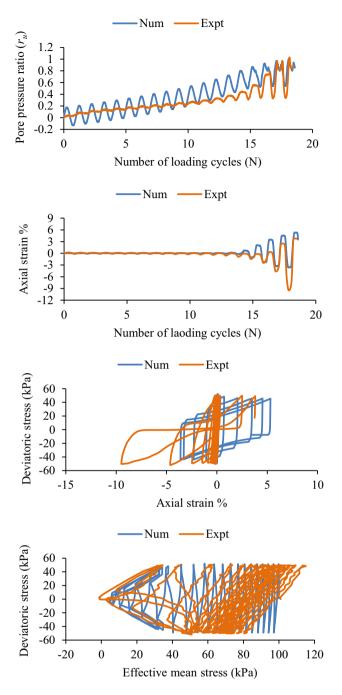
Figure 6. Comparison between experimental and numerical response for *S* 81.4, D_r 40,σ_c' 100 kPa, (*contrac* 0.03, *dilat1* 0.008, *dilat2* 0.2).

liquefac3 defines the maximum amount of biased perfectly plastic shear strain accumulated at each loading phase under biased shear loading conditions. The model can be used in plane strain and three-dimensional problems. The constitutive formulation of the model is based on the framework of multi-surface plasticity. It uses a Drucker-Prager yield criterion.

When used with regular solid elements, this model simulates drained response. On the other hand, when used

with solid-fluid fully coupled elements, it simulates an undrained response. Further, the partially drained response can also be simulated by defining a relatively large value of permeability. To date, literature mentions many soil models that can capture the hysteretic response of the saturated sandy soil under cyclic loading, but very few of them are capable of capturing a typical cyclic mobility response observed during undrained cyclic loading of saturated medium dense sand. The "PressureDependMultiYield" model used in this study captures not only the hysteric response but also typical cyclic mobility [21, 22].

The abovementioned model has a total of 15 constitutive parameters. These parameters are mainly divided into three categories: (1) Yield surface parameters, (2) Dilatancy parameters, and (3) Cyclic mobility parameters. Further details regarding these parameters can be found in Yang [19].

3.1 *Evaluation of constitutive parameters*

In the present study, small strain moduli are obtained from the expression suggested by Seed and Idriss [23]. Peak friction angle has been computed from the critical state friction angle by following the procedure recommended by Bolton [24]. Peak shear strain (0.1), Reference effective mean confining pressure (80 kPa) and Pressure dependency coefficient (0.5) are taken from the values recommended in OpenSees manual. Phase transformation angle is obtained from the isotropically consolidated undrained compression tests conducted in the present study. Dilatancy and cyclic mobility parameters for saturated and desaturated triaxial specimens are obtained by matching experimental results with numerical ones. It should be noted that triaxial specimen comprised of clean sand having a relative density of 40%.

Comparison between experimental and numerical response under monotonic and cyclic loading for the degree of saturation of 99% is shown in figures 3 and 4. It is observed that there is very well agreement between experimental and numerical results. It should be noted that several simulations were performed to reach the acceptable values of the dilatancy and cyclic mobility parameters. Further, a comparison between experimental and numerical response for the degree of saturation of 89.5% and 81.4%, under cyclic loading is shown in figures 5 and 6, respectively. There is reasonable agreement between experimental and numerical responses. The constitutive parameters for the degree of saturation of 99%, 89.5% and 81.4% are given in Table 4. It should be noted that constitutive parameters given in Table 4 are used in the site response analysis under scenario earthquakes which is discussed in next sections.

The lowest degree of saturation investigated in the present study is 81.4%. Literature states that for the clean sand with the degree of saturation as low as 70%, matric suction

Table 4. Constitutive parameters for various degrees of saturation

Degree of saturation %	99	89.5	81.4
Saturated unit weight (ton/m^3)	1.98	1.98	1.98
Small strain shear modulus, Gmax (kPa) at reference effective mean confining pressure of 80 kPa	7.83×10^4	7.83×10^4	7.83×10^4
Small strain shear modulus B (kPa) at reference effective mean confining pressure of 80 kPa	1.98×10^5	1.98×10^5	1.98×10^5
Friction angle (°)	34.14	34.14	34.14
Phase transformation angle (°)	26.56	26.56	26.56
Peak shear strain	0.1	0.1	0.1
Reference effective mean confining pressure (kPa)	80	80	80
pressDependCoe	0.5	0.5	0.5
contrac	0.4	0.2	0.03
dilat1	0.01	0.01	0.008
dilat2	0.20	0.20	0.20
liquefac1 (kPa)	10	10	10
liquefac2	0.02	0.02	0.02
liquefac3	1	1	1
Initial void ratio (e)	0.684	0.684	0.684

is negligible *i.e.,* around 3 - 4 kPa [25–27]. Therefore, in the present study in case of partly saturated sand, pore air pressure is assumed to be equal to the pore water pressure and thus, effect of matric suction has been neglected. Further, the constitutive model was originally developed for fully saturated sand. However, it should be noted that evolution of the pore pressure, axial strain and effective stress path depends upon the following constitutive parameters: *contrac*, *dilat1*, *dilat2*, *liquefac1*, *liquefac2*, *liquefac3*. Conventionally, these parameters are evaluated by matching the numerical response with the experimental one and same has been followed in the present study. What is crucial here is, an accurate evolution of pore pressure and axial straining. From figures 5 and 6, it is observed that there is reasonably well agreement between numerical and experimental pore pressure and axial strain evolution for partly saturated specimen. This implies that the constitutive model can be successfully used to simulate the cyclic response of the partly saturated soil as well.

4. Development of a numerical model for site response analysis

4.1 *Finite element discretization*

The thickness of the soil domain is 30 m, and the ground surface is assumed to be horizontal. Soil domain has been modelled adopting the shear beam approach [18]. In this approach, nodes at the same level are connected with an equal degree of freedom constraint in the horizontal and vertical direction. This simulates the vertical propagation of the horizontal shear wave. The finite element mesh along with boundary condition details is shown in figure 7

Bedrock is assumed to be at the base of the soil domain. It is worth noting here that geometry under consideration is 2-D, but the analysis is 1-D. Further, the domain is discretized into four node quadUP element. This is a plane strain element incorporating bilinear isoparametric formulation. This element successfully simulates the response of coupled solid-fluid material when subjected to dynamic loading [20].

It has been suggested by Kuhlemeyer and Lysmer [28] that the dimension of the finite element in the direction of the wave propagation should be such that the shortest wavelength also passes effectively. They suggested that this dimension should be one-eighth to one-tenth of the shortest wavelength, which is likely to pass through the medium. It is a well-established fact that the maximum shear wave frequency of engineering interest is 20 Hz. Shear waves above this frequency carry negligible energy [29]. Further, shear wave velocity for clean sand of relative density of 40% was found to be in the range of 190 m/sec to 250 m/sec at an effective confining pressure of 100 kPa and 300 kPa, respectively, for degree of saturation spanning from 80% to 100% [30]. Thus, the maximum length of the vertical dimension of the quadUP element is given by the following equation (1)

$$l_{max} = \frac{\lambda_{min}}{10}$$
$$l_{max} = \frac{v_s}{10 f_{max}}$$
$$l_{max} = \frac{v_s}{200}$$
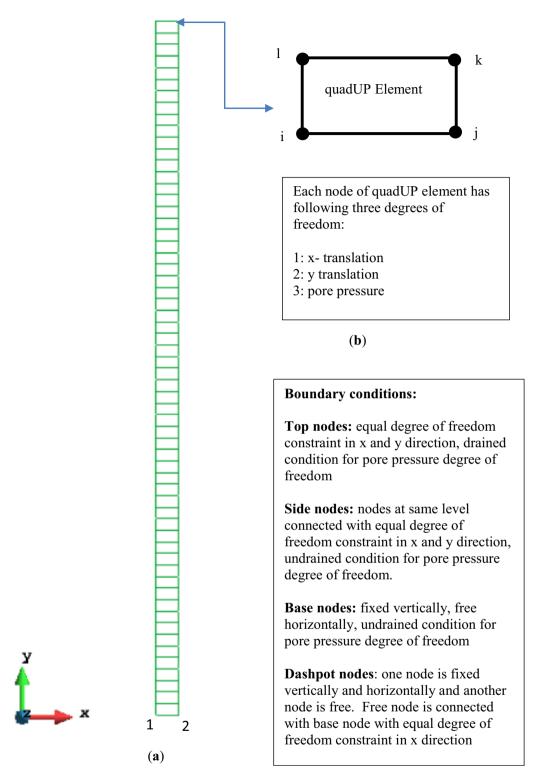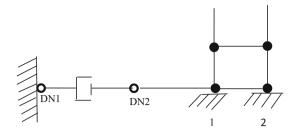$$l_{max} = \frac{190}{200} = 0.95 m$$

(1)

(b)

(a)

Figure 7. Details of: **a** finite element mesh and **b** quadUP element, along with boundary conditions.

In the present analysis, the vertical dimension of the quadUP element is 0.5 m << 0.95 m.

4.2 *Application of the earthquake load*

The earthquake load is applied at the base of the model in the horizontal direction in the form of equivalent shear

DN1 and DN2: dummy nodes created for dashpot

1 and 2: base nodes of quadUP domain

Coordinates of DN1, DN2 and DN3 are same.

Node DN2 is connected with node 1 with equal degree of freedom constraint in horizontal direction

Figure 8. Connection between dashpot and base nodes of the soil column.

force. Further, the radiation damping due to the finite rigidity of bedrock has also been modelled. The radiation damping and the equivalent shear force is computed from Eq. (2). The force induced by the vertical propagating shear wave at the soil-bedrock interface is given by the following equation [31].

$$F = -C\dot{u} + 2C\dot{u}_i \qquad (2)$$

In the above equation $\dot{u}$ is the total velocity of the particle at the soil-bedrock interface, which is sum of incident and reflected wave velocity, $\dot{u}_i$ is the velocity of the incident wave. Further, coefficient $= \rho V_s A$. Where, ρ is the mass density of bedrock, V_s is shear wave velocity for bedrock, and A is the tributary are of the node. In Eq. 2, the first term represents the radiation damping happening in the bedrock and the second term represents the equivalent shear force exerted by the incident wave onto the base of the soil column. It should be noted that the motion recorded at the outcrop is twice the motion anywhere within the body of the homogeneous, linear elastic and undamped half-space [29]. Therefore, while applying the recorded outcrop motion at the base of the model, it should be scaled down

by two and then applied. Further details can be found in [32–34].

Radiation damping is modeled by a viscous dashpot having coefficient C. A zero-length uniaxial material is defined between two dummy nodes to model the viscous dashpot as shown in figure 8. Further, one node of this zero-length element is connected to the base soil node in the horizontal direction with an equal degree of freedom constraint. The mass density of bedrock is assumed to be 2.5 ton/m^3, and shear wave velocity through bedrock is assumed to be 700 m/sec [34].

4.3 *Input motions*

The earthquake motions considered for the site response analysis are given in Table 5, along with their characteristics. The corresponding acceleration time history plots are shown in figure 9.

4.4 *Analysis stages in the site response analysis*

The analysis comprises three main stages: (1) *Gravity Analysis-Elastic*: The constitutive model is kept in elastic mode, self-weight is applied and analysis is performed. This simulates in-situ state of stress condition (initial state of stress). (2) *Gravity Analysis-Elastic Plastic*: The constitutive model is switched to the elastic-plastic mode and analysis is run for few pseudo times steps. This step is essential to adjust the state of stress given by step 1 on or within the outermost yield surface [20]. (3) *Dynamic Analysis-Elastic Plastic*: In this stage, earthquake load is applied and analysis is performed. During this stage, material model is in elastic-plastic state.

5. Results and discussion

Soil domain has been subjected to earthquake motions mentioned in Section 4.3, and the parametric study has been carried out. It should be noted that the water table is assumed at the ground surface and the boundary condition for the pore fluid pressure at the ground surface is set to be drained as mentioned in the figure 7. Liquefaction

Table 5. Characteristics of the input earthquake records

Earthquake	Station and Component	Magnitude	Duration (sec)	Peak acceleration (g)	Time of Peak acceleration(sec)
Bhuj (2001)	Ahmedabad N78E	7.0	133.525	− 0.106	46.940
Chamoli (1999)	Gopeshwar N20E	6.6	24.320	− 0.359	4.660
Uttarkashi (1991)	Bhatwari N85E	7.0	36.140	0.252	4.260
India Burma border (1988)	Berlongfer N14W	7.2	119.68	− 0.343	29.300

Bhuj (2001) Ahmedabad N78E

Chamoli (1999) Gopeshwar N20E

Uttarkashi (1991) Bhatwari N85E

India-Burma (1988) Berlongfer N14W

Figure 9. Acceleration time histories of input motions.

Figure 10. Effect of permeability on pore pressure evolution with time (input motion: Bhuj 2001 earthquake).

resistance of the soil, measured in terms of pore pressure ratio, for saturated and partly saturated soils has been investigated. For this purpose, the constitutive models evaluated in Section 3 are used. Effect of permeability and thickness of partly saturated zone on liquefaction resistance has also been looked into.

5.1 Effect of permeability on the liquefaction resistance

5.1.1 At depth of 5 m

In this section, the effect of permeability on the response of the soil domain developed in Section 4 has been
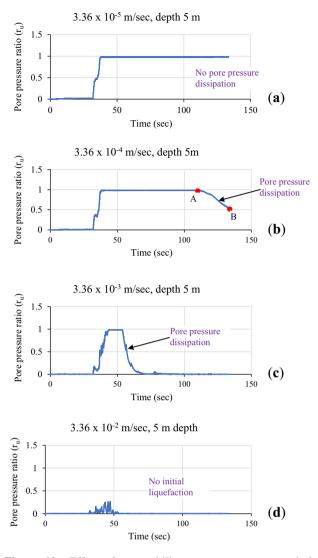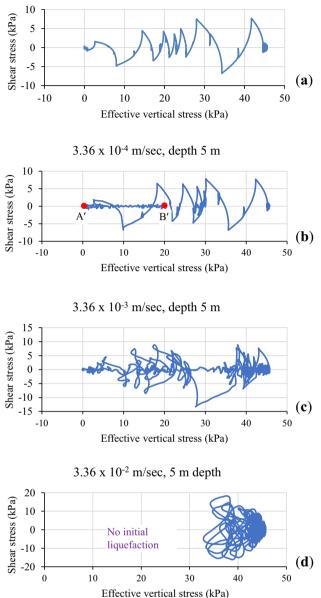
investigated. The soil domain is subjected to Bhuj earthquake 2001. The values of coefficient of permeability considered are: 3.36×10^{-5}, 3.36×10^{-4}, 3.36×10^{-3} and 3.36×10^{-2} m/sec. Further, the relative density of the soil is 40%, and the degree of saturation is 99%. Effect of permeability on pore pressure evolution, effective stress path, acceleration evolution and stress-strain curve, at a depth of 5 m, is shown in figures 10, 11, 12, 13.
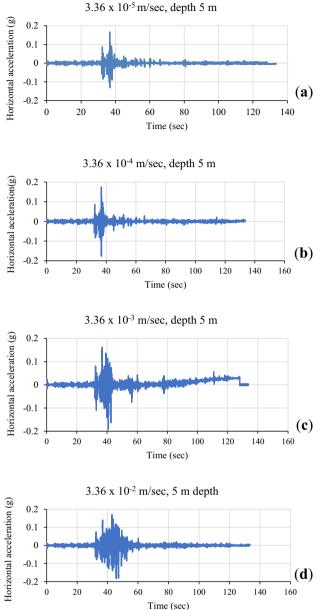
For the coefficient of permeability of 3.36×10^{-5} m/sec, the pore pressure ratio becomes one at around 38.5 seconds and remains constant throughout the shaking. This implies that soil undergoes initial liquefaction at around 38.5 seconds and remains in a liquified state throughout the shaking. However, in the case of 3.36×10^{-4} m/sec, the pore pressure ratio attains value one at around 39.0 seconds, remains constant up to 110 seconds and then onward starts decreasing. This implies that soil undergoes liquefaction at

Figure 11. Effect of permeability on effective stress path (input motion: Bhuj 2001 earthquake).

Figure 12. Effect of permeability on acceleration evolution (input motion: Bhuj 2001 earthquake).

around 39.0 seconds, remains in the liquefied state till 110 seconds, and then there is the reduction in the pore pressure ratio owing to pore pressure dissipation. The pore pressure dissipation is shown by segment AB in figure 10b, and the corresponding increase in the effective stress is shown by part A′B′ in figure 11b. In the case of 3.36×10^{-3} m/sec, excess pore pressure becomes one at around 42 seconds, starts dropping after 52.5 seconds and eventually becomes zero. In the last case, pore pressure attains its maximum value of $0.25 \ll 1.0$ at 47.0 seconds and immediately there onward starts decreasing. Thus, in the last case, the soil did not undergo liquefaction. From the above discussion, it can be inferred that increase in the permeability: (a) reduces the

generation of excess pore pressure (b) expedites the pore pressure dissipation (c) reduces the time span over which soil remains in a liquefied state.

Peak horizontal acceleration is observed to happen around 37, 37, 41 and 46 second for coefficient of permeability of 3.36×10^{-5}, 3.36×10^{-4}, 3.36×10^{-3} and 3.36×10^{-2} m/sec, respectively. Peak absolute acceleration is found to be 0.166 g, 0.176 g, 0.193 g and 0.183 g for coefficient of permeability of 3.36×10^{-5}, 3.36×10^{-4}, 3.36×10^{-3} and 3.36×10^{-2} m/sec, respectively. Thus, with the increase in the permeability, motion got amplified. It should be noted that the peak acceleration for all cases lies between -0.2 g and 0.2 g, as seen in figure 12. From

3.36 x 10⁻⁵ m/sec, depth 5 m

(a)

3.36 x 10⁻⁴ m/sec, depth 5 m

(b)

3.36 x 10⁻³ m/sec, 5 m depth

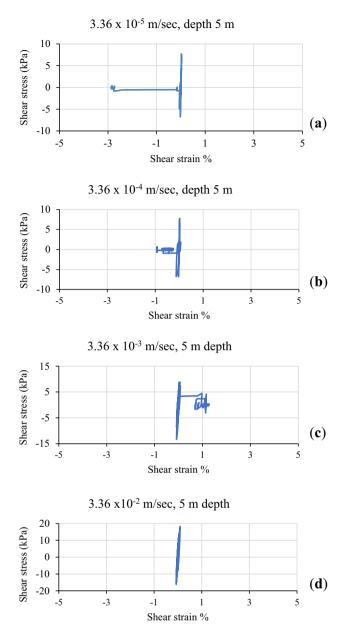**(c)**

3.36 x10⁻² m/sec, 5 m depth

(d)

Figure 13. Effect of permeability on stress-strain curve (input motion: Bhuj 2001 earthquake).

the shear stress-shear strain curve shown in the figure 13, it is observed that maximum shear strain is $- 3\%, - 1\%$, 1.25% and 0.1%, for permeability of 3.36×10^{-5}, 3.36×10^{-4}, 3.36×10^{-3} and 3.36×10^{-2} m/sec, respectively. Thus, the increase in the permeability reduces the shear straining.

5.1.2 *Along the entire thickness of the soil domain*

To understand the effect of coefficient of permeability on the liquefaction resistance along the entire 30 m thickness of the soil domain, maximum pore pressure ratio profile,

maximum horizontal acceleration profile and residual horizontal displacement profile along the thickness of the 30 m are plotted in figure 14. The maximum pore pressure ratio comprises the maximum pore pressure ratio at the given dept during the shaking. Maximum horizontal acceleration profile comprises maximum absolute acceleration at the given depth during the shaking. Residual horizontal displacement is the displacement at the end of shaking relative to the base. Thus, residual horizontal displacement is permanent horizontal displacement. From the maximum pore pressure ratio profile, it is observed that for the first two permeabilities, the soil between depth of 0 m and 27 m undergoes liquefaction and remains non-liquefied from 27 m to 30 m (segment PQ in figure 14a). For third permeability, the soil between depth of 0 m and 17 m liquefies and remains non-liquified between 17 m and 30 m (segment AB in figure 14a). However, in case of last permeability, no liquefaction is observed throughout the entire thickness of the soil domain. Further, the maximum pore pressure ratio is less than 0.5 << 1.0. Further, the pattern of residual horizontal displacement is similar for first two permeabilities and their values are also close. It should be noted that the residual horizontal displacement over the non-liquefied zone i.e., from 27 m to 30 m (segment P′Q′ in figure 14b), is zero. The residual horizontal displacement for third permeability is observed to be zero over the non-liquefied zone, i.e., from 17 m to 30 m (segment A′B′ in figure 14c). The pattern of residual horizontal displacement for the third case is distinct from the first two. The residual horizontal displacement for the last permeability, i.e., 3.36 $\times 10^{-2}$ m/sec, is found to be almost zero throughout the thickness of the soil domain. This is so because, in this case, the soil did not liquefy along with the entire thickness. It should be noted that the maximum residual horizontal displacement occurred between depth of 5 and 10 m as seen in figure 14b and c. Further, residual horizontal displacement at the ground surface is maximum for the smallest permeability, 3.36 $\times 10^{-5}$ m/sec.

From the maximum horizontal acceleration profile, it is observed that the acceleration lies in the range of 0.1 g to 0.3 g for all cases. Amplification factor at 0 m, 5 m and 10 m depth is given in figure 15. The amplification factor is the ratio of maximum acceleration at a given depth to the maximum input acceleration. From this figure, it is observed that the amplification factor is above 1 for all cases and at all three depths. Further, with an increase in permeability, the amplification factor increases. This implies that motion gets amplified on the increase in permeability. The amplification factor at the ground surface lies between 1.1 and 2.30. Further, the amplification factor at a depth of 5 m lies between 1.5 and 1.8 and that at a depth of 10 m falls between 1.3 and 1.5.
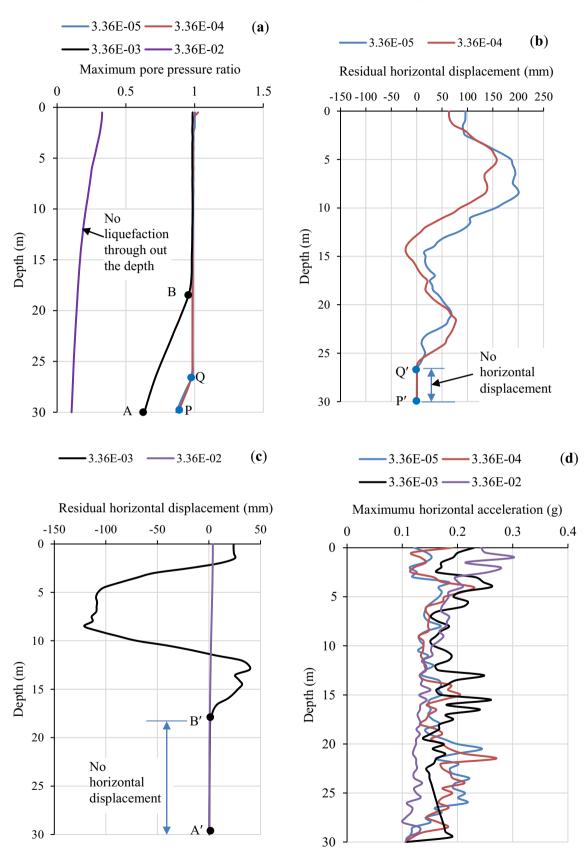
Figure 14. Envelopes for (**a**) maximum pore pressure ratio (**b**) and (**c**) residual horizontal displacement (**d**) maximum horizontal acceleration, (input motion: Bhuj 2001 earthquake).
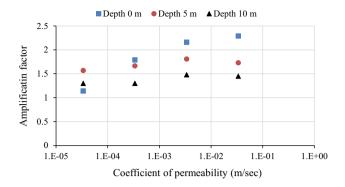
Figure 15. Effect of permeability on acceleration amplification, input motion Bhuj (2001), S 99.

5.2 *Effect of degree of saturation*

To begin with, two degrees of saturation are considered, *S* 99% and *S* 89.5%. The relative density of the soil is 40%, and input motion is Bhuj Earthquake 2001. The coefficient of permeability is 3.36×10^{-5} m/sec. In figure 16, maximum pore pressure ratio profile, maximum horizontal acceleration profile and residual horizontal displacement profile for *S* 89.5% and *S* 99% are shown. The thickness of the liquefied zone has been shown as L89.5 and L99 for *S* 89.5% and *S* 99%, respectively. As seen from figure 16a, L89.5 spans from 0 m to 18.5 m and L99 spans from 0 m to 27 m. Thus, when the degree of saturation was reduced from 99% to 89.5%, the thickness of the liquefied zone reduced by 8.5 m. In degree of saturation 89.5% liquefaction of the top zone is attributed partly to the acceleration amplification and partly to the relatively high degree of saturation. It is observed from figure 16b that over depth of 30 m to 18.5 m, input motion gets amplified to such an extent that it causes liquefaction of soil at 18.5 m and above. It should be noted that once the subsoil liquifies, it deampalifies the motion. This is clear from figure 16b. For *S* 99%, the motion gets amplified till 27 m, and this results in the liquefaction of the soil in the zone from 27 m to 19 m. Over this range, the average acceleration is almost constant. But above 19 m depth, average acceleration gets reduced. This is probably due to the liquefaction of the subsoil. Though there is deamplification of motion, the reduced acceleration is strong enough to cause liquefaction of the rest of the soil. Therefore, the soil above 19 m also gets liquefied for *S* 99%. Sharp peaks are observed in the acceleration profile for both *S* 89.5% and *S* 99%. This can be attributed to soil reaching a dense of critical state and regaining its stiffness and strength. Thus, liquefaction of the top zone is governed by three key factors: (1) liquefaction/non-liquefaction of subsoil, (2) motion amplification/deamplification and (3) degree of saturation.

Further, residual horizontal displacement is zero from 18.5 m to 30 m for *S* 89.5%, and it is zero from 17 m to 30 m for *S* 99%, as seen in figure 16c. It should be noted that this zone belongs to a non-liquefied state, as discussed

above. Moreover, residual horizontal displacement is observed to be maximum in between 5 m and 15 m in both cases. Residual horizontal displacement at the ground surface is around 100 mm and 50 mm for *S* 99% and *S* 89.5%, respectively. Thus, the decrease in the degree of saturation has main two effects: (1) reduction in the thickness of liquefied zone and (2) increase in the thickness of the zone of zero residual horizontal displacements.

5.3 *Effect of thickness of partly saturated zone*

To understand the effect of thickness and position of partly saturated zone on liquefaction resistance, parametric study for different thickness and position of the partly saturated zone was carried out. Total six cases are considered: Case (1) S 89.5 whole 30 m: this means that degree of saturation of the whole 30 m thickness is 89.5%, Case (2) S 89.5 top 15 m: this means that soil from 0 m to 15 depth has S 89.5% and soil from 15 m to 30 m depth has S 99%, (3) S 89.5 top 10 m: this means that soil from 0 m to 10 depth has S 89.5% and soil from 10 m to 30 m has S 99%, Case (4) S 89.5 top 5 m: this means that soil from 0 m to 5 depth has S 89.5% and soil from 5 m to 30 m depth has S 99%, Case (5) S 89.5 top 5 m to 10 m: this means that soil from 0 m to 5 m depth has S 99%, from 5 m to 10 m depth S 89.5% and from 10 m to 30 m depth S 99%. Case (6) S 99 whole 30 m: this means that degree of saturation of the whole 30 m thickness is 99.

The response of the above mentioned six cases under Bhuj earthquake 2001 for relative density of 40%, and the coefficient of permeability of 3.36×10^{-5} m/sec is shown in figure 17. It is observed from figure 17a that the top 5 m soil undergoes liquefaction for all cases. The maximum horizontal acceleration at the ground surface is observed to be in the range of 0.1 g and 0.2 g for all cases, as seen in figure 17b. It should be noted that the residual horizontal displacement, shown in Fig. figure 17c, is the function of (1) degree of saturation, (2) thickness and location of the partly saturated zone. To investigate the effect of further reduction in the degree of saturation, response for the degree of saturation of 81.4% for similar cases is shown in figure 18. It is observed that thickness of the non-liquefied zone is equal to the thickness of the partly saturated zone, except the first case, as seen in figure 18a. Further, acceleration at the ground surface falls in the range of 0.1 g to 0.2 g. Residual horizontal displacement at the ground surface of the fourth case is greater than that of the sixth case. This implies that residual horizontal displacement is the combined effect of degree of saturation, amplification, thickness and location of the partly saturated zone. The bar charts of maximum pore pressure ratio, amplification factor and residual horizontal displacement at a depth of 0 m, 5 m and 10 m for S 89.5% and S 81.4% under Bhuj 2001 motion are shown in figure 19.
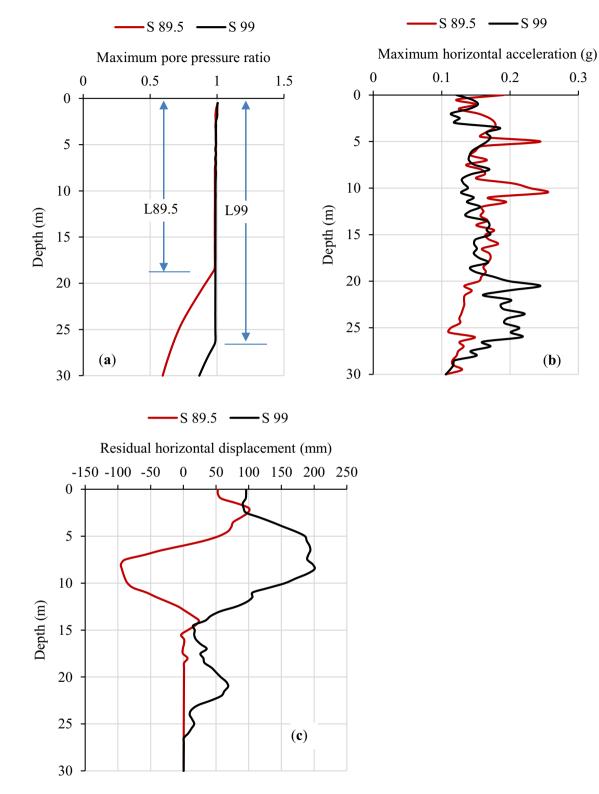
Figure 16. Effect of degree of saturation on liquefaction resistance, input motion Bhuj (2001).

The response of the soil domain with S 81.4%, the relative density of 40% and coefficient of permeability of 3.36 $\times$ 10^{-5} m/sec subjected to Chamoli earthquake (1999) having PGA $-$ 0.359 g is shown in figure 20. It is observed that the thickness of the non-liquefied zone is equal to the thickness of the partly saturated, except in the first case. It
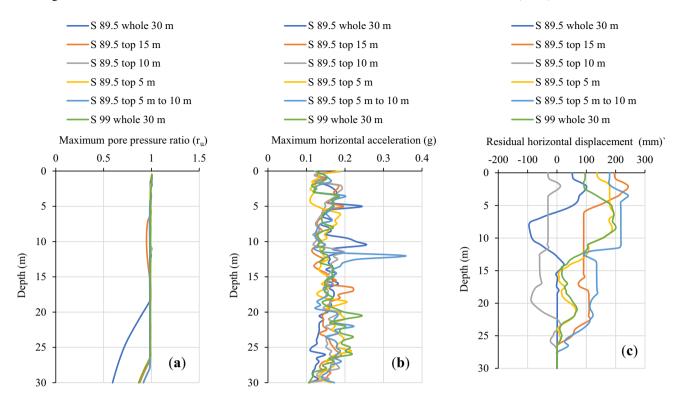
Figure 17. Liquefaction resistance of various desaturation zones, *S* 89.5, input motion Bhuj (2001).
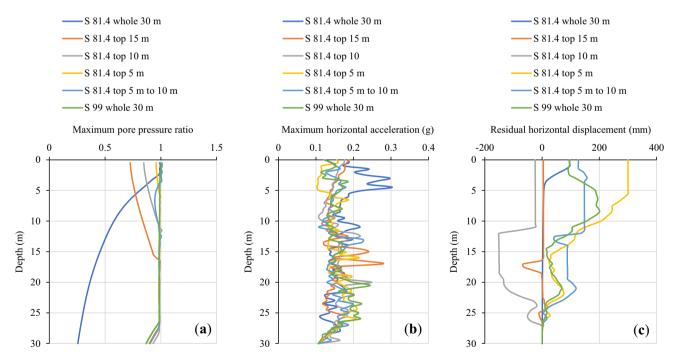
Figure 18. Effect of thickness of desaturation zone on liquefaction resistance, S 81.4, input motion Bhuj (2001).

should be noted that for the first case (S 81.4 whole 30 m), very large acceleration amplification within the soil body is observed. The maximum acceleration observed at a depth of 21 m is around 3 g. However, maximum acceleration at the ground surface is around 0.5 g. This is so because the soil in the range of 0 m to 5 m depth got liquefied, as seen
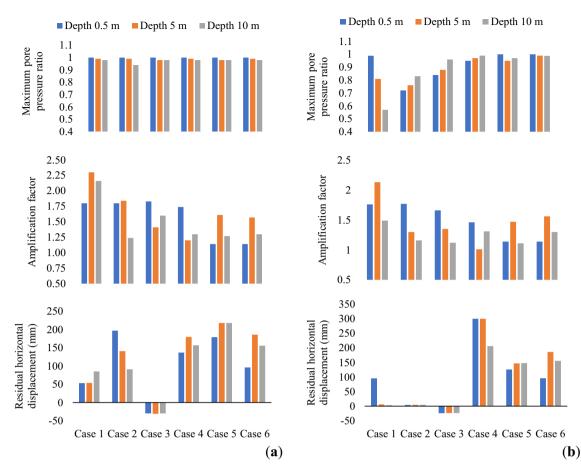
Figure 19. Effect of S 89.5 and 81.4% on various responses at three different depths, input motion Bhuj (2001): **a** S 89.5% and **b** S 81.4%.

from the maximum pore pressure ratio profile of figure 20. This resulted in deamplification of the motion. Response for S 81.4%, the relative density of 40% and coefficient of permeability of 3.36×10^{-5} m/sec subjected to India Burma border earthquake (1988) with PGA of -0.343 g is shown in figure 21. Again, it is observed that the thickness of the non-liquefied zone is equal to the thickness of the partly saturated zone, except the first case. Further, very high acceleration amplification within the soil body is observed for the first case. The maximum acceleration at a depth of 17 m is found to be 2.1 g. Soil above the 15 m depth got liquefied and resulted in deamplification of motion. That is why the maximum acceleration at the ground surface is just 0.2 g. The response of the same soil domain under the Uttarkashi earthquake (1991), having PGA of 0.252 g is shown in figure 22. Thickness of the non-liquefied zone is equal to the thickness of the partly saturated zone, except the first case. For the first case, soil above 5 m depth got liquefied. Further, large acceleration amplification within the soil body observed for Chamoli earthquake (1999), and India Burma border earthquake (1988) is not observed for the Uttarkashi earthquake (1991). One common observation for all four earthquake motions

for "S 81.4 whole 30 m" case is that soil near the ground surface got liquefied owing to the acceleration amplification resulted from non-liquefaction of the subsoil. Keeping this observation in view, it is suggested that desaturation of the entire thickness of 30 m should be avoided in practice.

5.4 *About acceleration amplification at the ground surface*

Amplification factor at the ground surface for relative density of 40% with the degree of saturation of 81.4% and coefficient of permeability of 3.36×10^{-5} m/sec under various earthquake records is given in Table 6. It is observed that the amplification factor is largest for the first case i.e., "S 81.4 whole 30 m" under all four earthquakes. As discussed in Section 5.3, for "S 81.4 whole 30 m" case soil at ground surface got liquefied owing to amplification caused by non-liquefaction of the subsoil. Therefore, desaturation of the entire thickness of 30 m is not recommended. The lowest amplification factor is observed for the sixth case i.e., "S 100 whole 30 m". For other cases of desaturation, the amplification factor at the ground surface lies between 0.32 and 1.76.
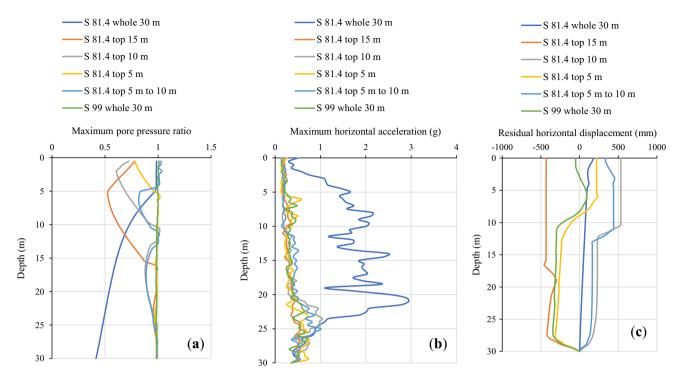
Figure 20. Liquefaction resistance of the soil, S 81.4, input motion Chamoli 1999.
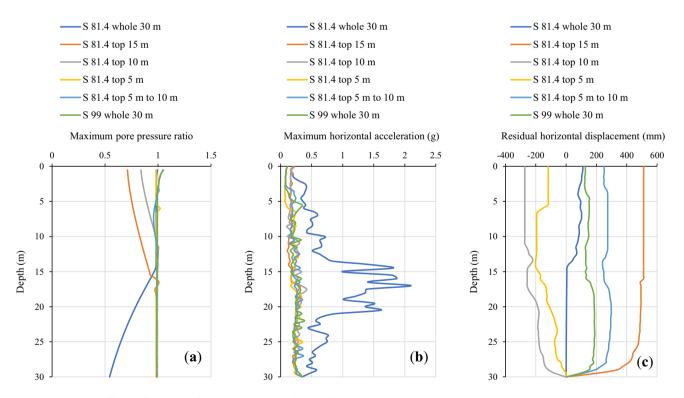

Figure 21. Liquefaction resistance of the soil, S 81.4, input motion India Burma border 1988.

Zeybek and Madabhushi [7] had performed centrifuges tests on air injected-desaturated sand of relative density of 40% having prototype thickness of 16.8 m. They found that for the degree of saturation of 79.5% when subjected to a sinusoidal acceleration of 0.18 g at a frequency of 0.72 Hz, the amplification factor was around 1.3. He *et al* [9]
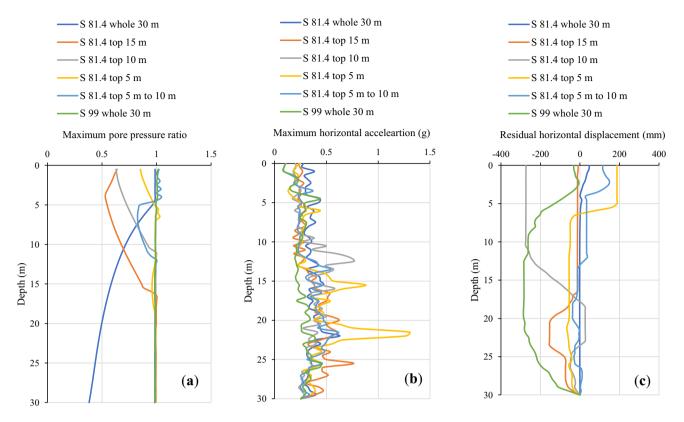
Figure 22. Liquefaction resistance of the soil, S 81.4, input motion Uttarkashi 1991.

Table 6. Amplification factor at the ground surface for various desaturation cases

	Amplification factor at the ground surface for:			
Desaturation case	Bhuj 2001 (− 0.106 g)	Chamoli 1999 (− 0.359 g)	India Burma 1988 (− 0.343 g)	Uttarkashi 1991 (0.252 g)
S 81.4 whole 30 m	1.76	1.40	0.66	1.10
S 81.4 top 15 m	1.76	0.60	0.63	0.91
S 81.4 top 10 m	1.66	0.58	0.57	0.79
S 81.4 top 5 m	1.46	0.74	0.33	0.98
S 81.4 top 5 m to 10 m	1.14	0.41	0.32	0.42
S 100 whole 30 m	1.14	0.38	0.32	0.42

conducted shaking table tests on the bio-desaturated model of the thickness of 0.30 m and found that for a model of the relative density of 40% with a degree of saturation of 80%, the amplification factor at the ground surface was 1.09. Input motion applied in their study had a peak acceleration of 0.15 g and a frequency of 2 Hz. From the present study, it is observed that the amplification factors observed for relative density of 40% at the degree of saturation of 81.4% under the Bhuj earthquake (peak acceleration 0.106 g) are close to those observed by the above mentioned researchers.

It is worth to note that Sitharam and Govindaraju [35] performed site response analysis of silty sand from Bhuj (India) under 2001 Bhuj earthquake and found that for the degree of saturation between 38.5% to 51.8%, the amplification factor could be as large as 20. Keeping in view the discussion held in this section so far, it can be concluded that desaturation up to the degree of saturation of 80% is adequate to achieve the twofold goal: (1) to prevent liquefaction and (2) to keep the amplification factor low.

5.5 *Investigation into very large accelerations*

In the previous sections it was observed that acceleration in the range of 2 g to 3 g occurred within the soil body for "S 81.4 whole 30 m" case when subjected to Chamoli (1999)
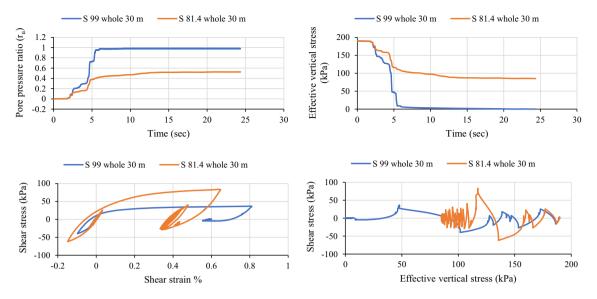
Figure 23. Pore pressure ratio evolution, variation of effective stress with time, stress-strain curves and effective stress path at a depth of 21 m, input motion Chamoli 1999.
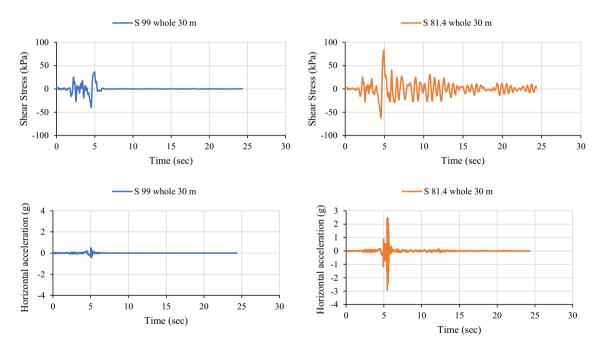

Figure 24. Variation of shear stress and horizontal acceleration with time at depth of 21 m, input motion Chamoli 1999.

and India Burma border (1988) earthquakes. In this section, the cause for this significantly large acceleration is investigated. For this purpose, various responses at a depth of 21 m for "S 99 whole 30 m" and "S 81.4 whole 30 m" under Chamoli earthquake are shown in figures 23, 24, 25. It is observed from figure 23 that at the end of 6 seconds, the pore pressure ratio becomes 1 in the case of S 99 while it is around 0.42 in the case of S 81.4. Generation of very high pore pressure in S 99 case reduces both effective stress and stiffness significantly. From the effective stress plot also, it

is clear that at the end of 6 seconds, effective vertical stress is 6 kPa for S 99, and it is around 106 kPa for S 81.4. As effective stress is significantly high in the later case, stiffness of the soil is also high, and this significantly high stiffness is responsible for large acceleration amplification. This is justified by the shear stress and acceleration evolution plots as well, shown in figure 24. It is observed from this figure that in the first case, shear resistance at the end of 5 seconds is around 40 kPa while in the later case it is 82 kPa. This high stiffness results in high acceleration and low
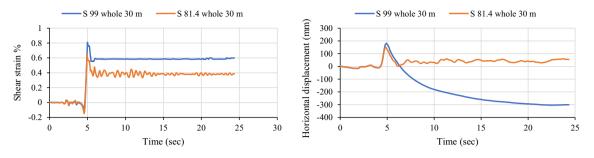
Figure 25. Shear strain and displacement evolution at depth of 21 m, input motion Chamoli 1999.

horizontal displacement in the later case. Horizontal displacement plots for both cases are is shown in figure 25. It is observed that around 5 second, there is a sudden rise in the displacement in both cases. After 5 second displacement significantly reduces and remain almost constant for S 81.4 case due to considerable stiffness whereas, in case of S 99, displacement changes its direction and achieves a very large value of around - 300 mm due to very low post liquefaction stiffness.

6. Practical implications of the present study

The present research reveals that reduction in the degree of saturation increases liquefaction resistance. Desaturation up to degree of saturation of 80% is found to be adequate to prevent liquefaction and simultaneously keep the acceleration amplification minimum. If the site under consideration is fully saturated and prone to liquefaction, the degree of saturation of such a site can be brought down by techniques such as air injection and microbial desaturation. Once the in-situ soil is desaturated, superstructure can be bult upon. In cases where superstructure already exists, controlled air injection technique shall be adopted. The air should be injected gradually and the vertical settlement of the structure should be carefully monitored [6]. Care shall be taken that the vertical settlement during air injection is within permissible limits. Alternative to the air injection is microbial desaturation. In this case there is no risk of unacceptable vertical settlement, however, the desaturation zone is likely to be narrow and shallow. The induced desaturation technique can also be adopted when the embankment rests on the liquefiable subsoil.

7. Conclusions

In the present study, undrained monotonic and cyclic triaxial tests for the degree of saturation of 99%, 89.5% and 81.4% were conducted. Experimental test results were employed to evaluate constitutive parameters for pressure dependent multi yield material model in OpenSees. Using these constitutive models, site response analysis was carried out for four scenario earthquakes. The major conclusions drawn from the present study are given below:a) Effect of permeability

Increase in the permeability had three main effects: (a) reduction in the generation of excess pore pressure, (b) faster dissipation of the pore pressure and (c) acceleration amplification. (d) Effect of degree of saturation

It was observed that reduction in the degree of saturation from S 99% to S 89.5% had minimal effect on the liquefaction resistance of soil, measured in terms of generation of excess pore pressure. However, when the degree of saturation was reduced to S 81.4%, a significant increase in the liquefaction resistance, measured in terms of generation of excess pore pressure, was observed. (c) Effect of thickness of partly saturated zone

(1) Degree of saturation of 89.5%: For given earthquake motion, the non-liquefaction zone is observed to be maximum for "S 89.5 whole 30 m" case. For other cases, it was observed that the thickness of the liquefaction zone is almost constant irrespective of the thickness of partly saturated zone. Acceleration at the ground surface falls in a narrow band.
(2) Degree of saturation of 81.4%: Effect of thickness of partly saturated zone is very pronounced for this degree of saturation. When the entire 30 m was considered to be partly saturated, part of the soil in the top 0 m to 15 m depth only liquefied depending on the input motion. For all other cases, the thickness of the non-liquefied zone is equal to the thickness of partly saturated zone.d) Effect of input acceleration

For S 81.4% case, very high acceleration amplification was observed within the soil domain in the case of Chamoli (1999) and India Burma Border (1988) earthquakes. Investigation revealed that this amplification was combined effect of input peak acceleration and significantly high stiffness of the soil owing to its non-liquefaction. However, at the ground surface, this acceleration was close to the acceleration observed for other cases. This happened due to

deamplification caused by liquefaction of the soil in the top region.

Declarations

Conflict of interest The authors have no conflicts of interest to declare.

References

[1] Idriss I M and Boulanger R 2008 Soil liquefaction during earthquakes. *EERI*

[2] Ishihara M, Okamura M and Oshita T 2003 Desaturating sand deposit by air injection for reducing liquefaction potential. *Pacific Conf. Earthq. Eng.*

[3] Pietruszczak S, Pande G N and Oulapour M 2003 A hypothesis for mitigation of risk of liquefaction. *Géotechnique* 53: 833–838. https://doi.org/10.1680/geot.2003.53.9.833

[4] Yegian M K, Eseller-Bayat E, Alshawabkeh A and Ali S 2007 Induced-partial saturation for liquefaction mitigation: experimental investigation. *J. Geotech. Geoenvironmental Eng.* 133: 372–380. https://doi.org/10.1061/(ASCE)1090-0241(2007)133:4(372)

[5] Takemura J, Igarashi R, Izawa J, Okamura M and Masuda M 2009 Centrifuge model tests on soil desaturation as a liquefaction countermeasure. *Proc. 17th Int. Conf. Soil Mech. Geotech. Eng. Acad. Pract. Geotech. Eng.* 1: 502–505. https://doi.org/10.3233/978-1-60750-031-5-502

[6] Zeybek A and Madabhushi S P G 2017 Influence of air injection on the liquefaction-induced deformation mechanisms beneath shallow foundations. *Soil Dyn. Earthq. Eng.* 97: 266–276. https://doi.org/10.1016/j.soildyn.2017.03.018

[7] Zeybek A and Madabhushi S P G 2016 Centrifuge testing to evaluate the liquefaction response of air-injected partially saturated soils beneath shallow foundations. *Bull. Earthq. Eng.* 1–18. https://doi.org/10.1007/s10518-016-9968-6

[8] Okamura M, Takebayashi M, Nishida K, Fujii N, Jinguji M and Imasto T et al. 2011 In-situ desaturation test by air injection and its evaluation through field monitoring and multiphase flow simulation. *J. Geotech. Geoenvironmental Eng.* 137: 643–652. https://doi.org/10.1061/(ASCE)GT.1943-5606.0000483

[9] He J, Chu J and Ivanov V 2013 Mitigation of liquefaction of saturated sand using biogas. *Géotechnique* 63: 267–275. https://doi.org/10.1680/geot.SIP13.P.004

[10] Marasini N P and Okamura M 2015 Air injection to mitigate liquefaction under light structures. *Int. J. Phys. Model Geotech.* 15: 129–140. https://doi.org/10.1680/jphmg.14.00005

[11] He J, Chu J and Liu H 2014 Undrained shear strength of desaturated loose sand under.pdf. *Soils Found* 54: 910–916

[12] Marasini N P and Okamura M 2015 Numerical simulation of centrifuge tests to evaluate the performance of desaturation by air injection on liquefiable foundation soil of light structures. *Soils Found.* 55: 1388–1399. https://doi.org/10.1016/j.sandf.2015.10.005

[13] Zhang B, Muraleetharan K K and Liu C 2016 Liquefaction of Unsaturated Sands. *Int. J. Geomech.* 16:D4015002(1-9). https://doi.org/10.1061/(ASCE)GM.1943-5622.0000605

[14] Chavan D, Sitharam T G and Anbazhagan P 2021 Liquefaction resistance and cyclic response of air injected-desaturated sandy soil. *Geotech. Geol. Eng..* https://doi.org/10.1007/s10706-021-01996-5

[15] Lade P V 2016 Triaxial testing of soils. Wiley, London

[16] Puzrin A M 2012 Constitutive modelling in geomechanics introduction. Springer, Berlin

[17] Bae S, Lagrava D, McGann C, Chandramohan R, Motha J and Bradley B 2017 QuakeCoRE OpenSees Training Workshop 2017 *Geotechnical Analysis in OpenSees*

[18] Parra-Colmenares E J 1996 *Numerical modeling of liquefaction and lateral ground deformation including cyclic mobility and dilation response in soil systems.* Rensselaer Polytechnic Institute, Troy, NY

[19] Yang Z 2000 N*umerical modeling of earthquake site response including dilation and liquefaction.* Columbia University

[20] Mazzoni S, Mckenna F, Scott M H and Fenves G L 2007 OpenSees Command Language Manual

[21] Elgamal A, Yang Z and Parra E 2002 Computational modeling of cyclic mobility and post liquefaction site response. *Soil Dyn. Earthq. Eng.* 22: 259–271

[22] Elgamal A, Yang Z and Parra E 2003 Modeling of cyclic mobility in saturated cohesionless soils. *Int. J. Plast.* 19: 883–905

[23] Seed H B and Idriss I M 1970 Soil Moduli and Damping Factors for Dynamic Analysis. Earthq Eng Res Center, *EERC 41*

[24] Bolton M D 1986 The strength and dilatancy. *Geotechnique* 36: 65–78

[25] Likos W J and Jaafar R 2013 Pore-scale model for water retention and fluid partitioning of partially saturated granular soil. *J. Geotech. Geoenviron. Eng.* 139: 724–737. https://doi.org/10.1061/(ASCE)GT.1943-5606.0000811

[26] Okamura M and Soga Y 2006 Effects of Pore Fluid Compressibility on Liquefaction Resistance of Partially Saturated Sand. *Soils Found.* 46: 695–700. https://doi.org/10.3208/sandf.46.695

[27] Unno T, Kazama M, Uzuoka R and Sentos N 2008 Liquefaction of unsaturated sand considering the pore air pressure and volume compressibility of the soil particle skeleton. *Soils Found* 48: 87–99. https://doi.org/10.3208/sandf.48.87

[28] Kuhlemeyer R L, Lysmer J 1973 Finite element method accuracy for wave propagation problems. *J. Soil Mech. Found. Div*, 99(Tech Rpt)

[29] Kramer S L 1996 Geotechnical Earthquake Engineering. PEARSON

[30] Kumar J and Madhusudhan B N 2012 Dynamic properties of sand from dry to fully saturated states. *Geotechnique* 62: 45–54. https://doi.org/10.1680/geot.10.P.042

[31] Joyner W B and Chen A T F 1975 Calculation of nonlinear ground response in earthquakes. *Bull. Seismol. Soc. Am.* 65: 1315–1336

[32] Kolay C 2009 *Seismic analysis of bridge abutment-soil system.* M.Tech. thesis, Indian Institute of Technology Kanpur, India

[33] Chavan D 2012 *Permanent Displacement of Nailed Soil Slopes Subjected to Earthquake Loading.* M.Tech. thesis, Indian Institute of Technology Kanpur

[34] McGann C and Arduino P 2011 Site Response Analysis of a Layered Soil Column (Total Stress Analysis). https://opensees.berkeley.edu/wiki/index.php/Site Response Analysis of a Layered Soil Column (Total Stress Analysis)

[35] Sitharam T G and Govindaraju L 2004 Geotechnical aspects and ground response studies in Bhuj earthquake, India. *Geotech. Geol. Eng.* 22: 439–455. https://doi.org/10.1023/B:GEGE.0000025045.90576.d3